

Dynamical instability of a Bose-Einstein condensate with higher-order interactions in an optical potential through a variational approach

E. Wamba,^{1,2} S. Sabari,³ K. Porsezian,³ A. Mohamadou,^{4,5} and T.C. Kofané¹

¹*Department of Physics, Faculty of Science, University of Yaoundé I, P.O. Box 812, Yaoundé, Cameroon*

²*African Institute for Mathematical Sciences, 6 Melrose Road, Muizenberg, 7945, South Africa*

³*Department of Physics, Pondicherry University, Puducherry 605014, India*

⁴*Department of Physics, Faculty of Science, University of Douala, P.O. Box 24157, Douala, Cameroon*

⁵*The Abdus Salam International Centre for Theoretical Physics,
P.O. Box 586, Strada Costiera 11, I-34014, Trieste, Italy*

We investigate the dynamical instability of Bose-Einstein condensates (BECs) with higher-order interactions immersed in an optical lattice with weak driving harmonic potential. For this, we compute both analytically and numerically a modified Gross-Pitaevskii equation with higher-order nonlinearity and external potentials generated by magnetic and optical fields. Using the time-dependent variational approach, we derive the ordinary differential equations for the time evolution of the amplitude and phase of modulational perturbation. Through an effective potential, we obtain the modulational instability condition of BECs and discuss the effect of the higher-order interaction in the dynamics of the condensates in presence of optical potential. We perform direct numerical simulations to support our analytical results, and good agreement is found.

PACS numbers: 05.45.-a, 03.75.Kk, 03.75.Lm, 05.30.Jp

I. INTRODUCTION

Over the past two decades, the dynamics and properties of Bose-Einstein condensates (BECs) in optical lattices (OLs) have been intensively investigated both experimentally [1–3] and theoretically [4–7]. In these works, the OL created by the interference of laser beams induces a periodic potential that traps the bosonic atoms. The properties of the atoms are characterized by the depth and period of the optically induced potential. An interesting feature of this lattice potential is that its intensity can be modulated from very weak to very strong [1]. BECs in periodic potentials have been used to investigate many physical phenomena, such as Josephson effect [8], Bloch oscillations [1, 9, 10], Landau-Zener tunneling [11], solitons [12], quantum phase transitions of the Mott insulator type [13], superfluid and dissipative dynamics [14], phase diagram [15], and nonlinear dynamics of a dipolar [16] or spinor BEC [17].

Most findings of experiments in BECs are reproduced and described by the theoretical model based on the nonlinear mean-field Gross-Pitaevskii (GP) equation [18]. The nonlinear term arises in the GP equation due to the effect of the inter-atomic interaction in the condensate which is described by the s -wave scattering length, a_s . The interaction strength can be controlled by using different experimental techniques. Notably, the strength and sign of the atomic scattering length can be varied by tuning the external magnetic field near Feshbach resonances [19]. When the sign is positive, the interaction in the BEC is repulsive. In the presence of OL, such interaction can give rise to stable localized matter-wave states in the form of gap solitons. The BEC gap soliton was predicted theoretically [20–22] and demonstrated experimentally [3]. Gap solitons are represented by stationary solutions to the respective GP equation, with the eigen-

value (chemical potential) located in a finite bandgap of the OL-induced spectrum [23]. In BECs with attractive interactions ($a_s < 0$), solitons realize the ground state of the condensate. Such solitons were created in condensates of ^7Li [24] and ^{85}Rb [25] atoms, with the sign of the atomic interactions switched to attraction by means of the Feshbach-resonance technique. In the presence of a periodic potential, such solitons should exist too as first shown in the context of optical setting [6], and later demonstrated in detail in the framework of BECs through a GP equation [26, 27]. However, the simple mean-field GP equation is less convenient in some contexts. Higher-order terms in the expansion of the phase shifts at low momenta, determined by the effective range, the shape parameter etc., give corrections to the simple GP equation. It has been shown that the critical number of condensed atoms needed for stability, the chemical potential, the condensate profiles and the energy levels of a harmonically trapped BEC strongly depend on the higher-order scattering term when the scattering length approaches zero [28]. Furthermore, because the higher-order interactions is determined by the shape parameter we can expect that the higher-order interactions would strongly be affected by the trap potential. Then studying the dynamics of BECs considering the presence of higher-order interactions becomes relevant especially in the case of narrow resonances.

In many dispersive systems described by nonlinear wave equations, it appears the general phenomenon of modulational instability (MI). For nonlinear systems in periodic potentials, the MI is usually referred to as the *dynamical instability* since it is directly connected to the dynamic equation which describes the system [29]. It occurs when the eigenspectrum of the excitations of the system exhibits complex frequencies. In this case, due to the interplay between nonlinearity, dispersion and periodic-

ity, arbitrary small perturbations of the wave function may grow exponentially, eventually leading to the destruction of the initial state [29–33]. MI has been demonstrated both experimentally [32, 34–36] and theoretically [37–39]. Recently, many investigations have been devoted to the MI of both single-component BECs and double-species BECs in optical lattices [29, 32, 33, 40–42]. Moreover, the studies with relation to the MI have also attracted much interest, as the MI is an indispensable mechanism for understanding the relevant dynamic processes in the BEC systems, which include domain formation [43, 44], generation and propagation of solitonic waves [45, 46] and quantum phase transition [47], etc. The study of MI is usually conducted by means of the standard linear stability analysis, which unfortunately cannot help efficiently in the context of OL. In this paper we reexamine the MI in the nonlinear Schrödinger (NLS) equation with the effect of periodic potential and higher-order nonlinearity with the help of time-dependent variational approach and numerical calculations.

The paper is organized as follows: in Sec. II, we present the theoretical model that describes the condensates with higher-order nonlinearity in OL. Sec. III is devoted to the analytical framework in which we derive the MI conditions of the system through the time-dependent variational approach and predict the dynamics of the system in both cases of attractive and repulsive interactions. Then, in Sec. IV, we perform direct numerical integrations to check the validity of the MI conditions found by analytical methods and study the interplay between higher-order nonlinearity and optical potential. Sec. V summarizes our results and conclude the work.

II. THEORETICAL MODEL

In the ultracold regime where the temperature is much smaller than the critical temperature for condensation, a Bose gas may obey the $T = 0$ formalism. The higher-order effects in the two-body scattering dynamics can be captured by an energy functional [48, 49] which allows the derivation of the following generalized (or modified) GP equation [50, 51]

$$i\hbar \frac{\partial \psi(\mathbf{r}, t)}{\partial t} = -\frac{\hbar^2}{2m} \nabla^2 \psi(\mathbf{r}, t) + V_{\text{ext}}(\mathbf{r}) \psi(\mathbf{r}, t) + g_0 |\psi(\mathbf{r}, t)|^2 \psi(\mathbf{r}, t) + \eta \nabla^2 (|\psi(\mathbf{r}, t)|^2) \psi(\mathbf{r}, t). \quad (1)$$

In Eq. (1) \hbar is the reduced Planck's constant, m is the mass of the boson, and g_0 is the strength of the two-body inter-atomic interactions defined by $g_0 = 4\pi\hbar^2 a_s/m$, with a_s being the s -wave scattering length. **The strange nonlinear term which depends on the Laplacian of the number density is the so-called *residual nonlinearity* [51]. It describes the shape-dependent confinement correction of the two-body collision**

potential. The parameter η is the higher-order scattering coefficient which depends on both the s -wave scattering length and the effective range for collisions [48–50]. This parameter reads $\eta = g_0 g_2$, where g_2 is defined by $g_2 = a_s^2/3 - a_s r_e/2$, with r_e being effective range. The model in Eq. (1) was derived and explained in [50] (and Refs. therein) for any general external potential $V_{\text{ext}}(\mathbf{r})$, and the physical meaning of the residual nonlinearity was discussed in full detail. When the Bose gas with higher-order interaction (HOI) is immersed in a trap consisting of an OL driven by a highly elongated harmonic trap [31, 32], the dynamics of the condensate is governed by the following modified GP equation

$$i\hbar \frac{\partial \psi(\mathbf{r}, t)}{\partial t} = -\frac{\hbar^2}{2m} \nabla^2 \psi(\mathbf{r}, t) + \frac{m}{2} (\omega_\perp^2 \rho^2 + \omega_x^2 x^2) \psi(\mathbf{r}, t) + V_{\text{OL}}(x) \psi(\mathbf{r}, t) + g_0 |\psi(\mathbf{r}, t)|^2 \psi(\mathbf{r}, t) + \eta \nabla^2 (|\psi(\mathbf{r}, t)|^2) \psi(\mathbf{r}, t), \quad (2)$$

where ω_\perp and ω_x , respectively, are the radial and longitudinal frequencies of the anisotropic trap ($\omega_\perp \neq \omega_x$), and $\rho = \sqrt{y^2 + z^2}$ denotes the radial distance. The OL potential is applied only in the axial direction, such as to have $V_{\text{OL}}(x) = V_{\text{max}} \cos^2(\kappa x)$, with V_{max} and κ being the effective depth and the wave number of the optical potential, respectively.

In the case of elongated or cigar-shaped condensate ($\omega_\perp \gg \omega_x$), we can make the change $\psi(\mathbf{r}, t) = \phi_0(\rho) \phi(x, t)$, where $\phi_0 = \sqrt{\frac{1}{\pi a_\perp^2}} \exp(-\frac{\rho^2}{2a_\perp^2})$ with $a_\perp = \sqrt{\hbar/m\omega_\perp}$, is the ground state of the radial equation

$$-\frac{\hbar^2}{2m} \nabla_\rho^2 \phi_0 + \frac{m}{2} \omega_\perp^2 \rho^2 \phi_0 = \hbar \omega_\perp \phi_0. \quad (3)$$

Then, multiplying both sides of the GP Eq. (2) by ϕ_0^* and integrating over the radial variable ρ , we obtain a quasi-1D GP equation that reads:

$$i\hbar \frac{\partial \phi(x, t)}{\partial t} = \left[-\frac{\hbar^2}{2m} \nabla_x^2 + \left(\frac{m}{2} \omega_x^2 x^2 + V_{\text{max}} \cos^2(\kappa x) \right) \right] \phi + \left[\frac{g_0}{2\pi a_\perp^2} |\phi|^2 + \frac{\eta}{2\pi a_\perp^2} \nabla_x^2 |\phi|^2 \right] \phi. \quad (4)$$

In most cases, the above Eq. (4) is used in a dimensionless form [52–54]. For this purpose we need to introduce the following change of variables: $t \sim t\nu$, $x \sim x\kappa$, $\phi \sim \phi \sqrt{2a_{s0}\omega_\perp/\nu}$, where $\nu = E_R/\hbar$, $\alpha = \omega_x^2/4\nu^2$ and $E_R = \hbar^2 \kappa^2/2m$. Then, we come to the following normalized 1D GP equation with harmonic and optical potentials:

$$i \frac{\partial \phi(x, t)}{\partial t} = -\nabla_x^2 \phi + (\alpha x^2 + V_s \cos^2(x)) \phi + g |\phi|^2 \phi + g\sigma \nabla_x^2 |\phi|^2 \phi, \quad (5)$$

where $\nabla_x^2 = \frac{\partial^2}{\partial x^2}$, $V_s = V_{max}/E_R$, $\sigma = g_2\kappa^2$, $a_s = g a_{s0}$, with a_{s0} being the constant scattering length, $g = \pm 1$ is the sign of the scattering length. Some special cases of that equation have been considered in previous works [55, 56]. In order to get the analytical condition that may allow to examine the MI of BECs in the system, we first need to find for Eq. (5) an expression with less space-dependent coefficients. We begin with a modified lens-type transformation which consists in setting [57]

$$\phi(x, t) = \frac{1}{\sqrt{l(t)}} \tilde{\psi}(\tilde{x}, \tilde{t}) \exp(i f(t) x^2). \quad (6)$$

In this expression, we choose $l(t) = |\cos(2\sqrt{\alpha}t)|$, $\tilde{x} = \frac{x}{l(t)}$, $\tilde{t}(t) = \frac{1}{2\sqrt{\alpha}} \tan(2\sqrt{\alpha}t)$, and $f(t) = -\frac{\sqrt{\alpha}}{2} \tan(2\sqrt{\alpha}t)$. The rescaling signals the existence of negative \tilde{t} and is valid for any $t \neq \frac{(2n+1)\pi}{4\sqrt{\alpha}}$ (where n is a positive integer) in the t - \tilde{t} plane. We consider the case where t goes from zero to $\pi/(4\sqrt{\alpha})$ to ensure a continuous variation of \tilde{t} from zero to infinity. Let us note in passing that the length scale $l(t)$ can be written in terms of the new time as $l(\tilde{t}) = 1/\sqrt{1+4\alpha\tilde{t}^2}$. For simplicity, we will drop the tildes in what follows. Then Eq. (5), in terms of the new variables x and t , is reduced to

$$i \frac{\partial \psi(x, t)}{\partial t} = -\nabla_x^2 \psi(x, t) + V_0(t) \cos^2(x) \psi(x, t) + s(t) |\psi(x, t)|^2 \psi(x, t) + \eta(t) \nabla_x^2 |\psi(x, t)|^2 \psi(x, t), \quad (7)$$

where $V_0(t) = V_s (1+4\alpha t^2)^{-1}$, $s(t) = g (1+4\alpha t^2)^{-1/2}$ and $\eta(t) = \sigma g (1+4\alpha t^2)^{1/2}$ are the new rescaled strengths of OL, two-body and HOIs. The 1D GP Eq. (7) can be more easily handled through variational methods.

III. ANALYTICAL RESULTS

A. Variational approximation and instability criteria

For many physical systems, the variational approximation method has been found to be an indispensable tool in the investigation of dynamical properties. Here, we use a time-dependent variational approach to examine the MI of BECs with HOI trapped in optical potential. As applied in many works [58, 59], the first step of the process consists in finding the Lagrangian density that may generate the governing Eq. (7). Such density reads

$$\mathcal{L} = \frac{i}{2} \left(\frac{\partial \psi}{\partial t} \psi^* - \frac{\partial \psi^*}{\partial t} \psi \right) - |\nabla_x \psi|^2 - V_0(t) \cos^2(x) |\psi|^2 - \frac{s(t)}{2} |\psi|^4 - \frac{\eta(t)}{2} |\psi|^2 \nabla_x^2 (|\psi|^2). \quad (8)$$

It is easy to show that an exact solution of the NLS Eq. (7) in the absence of optical potential is a wave of the

form

$$\psi(x, t) = A_0 \exp \left[i \left(kx - k^2 t - A_0^2 \int_0^t s(t') dt' \right) \right]. \quad (9)$$

Then we may use, as variational ansatz for the wavefunction of the condensate, a MI-motivated trial wave function given by the following ansatz

$$\begin{aligned} \psi(x, t) = & \left\{ A_0 + a_1(t) \exp[i(qx + b_1(t))] + \right. \\ & \left. a_2(t) \exp[i(-qx + b_2(t))] \right\} \\ & \times \exp \left[i \left(kx - k^2 t - A_0^2 \int_0^t s(t') dt' \right) \right]. \end{aligned} \quad (10)$$

This trial wave function may be substituted into the Lagrangian density which may be integrated over the entire space to obtain the effective Lagrangian. A tricky way of computing the effective Lagrangian for this type of problem is to consider a circular (1D) geometry, which imposes periodic boundary conditions on the wavefunction $\psi(x, t)$ and integration limits $0 \leq x < 2\pi$. This causes the quantization of the wave numbers, i.e. $k, q = 0, \pm 1, \pm 2, \pm 3, \dots$. In this new geometry, calculating the effective Lagrangian yields

$$\begin{aligned} L_{\text{eff}} = & -\pi \left\{ A_0^2 [V_0 - A_0^2 s(t)] \right. \\ & + a_1^2 \left[2q(q + 2k - A_0^2 q \eta(t)) + s(t)(2A_0^2 + a_1^2) + 2\dot{b}_1 + V_0 \right] \\ & + a_2^2 \left[2q(q - 2k - A_0^2 q \eta(t)) + s(t)(2A_0^2 + a_2^2) + 2\dot{b}_2 + V_0 \right] \\ & + 4a_1 a_2 s(t) [a_1 a_2 + A_0^2 \cos(b_1 + b_2)] \\ & \left. - 4a_1 a_2 q^2 \eta(t) [2a_1 a_2 + A_0^2 \cos(b_1 + b_2)] \right\}. \end{aligned} \quad (11)$$

The expression of this effective Lagrangian is such that the pair $\{b_1(t), b_2(t)\}$ may be interpreted as the set of generalized coordinates of the system, while the pair $\{A_1(t), A_2(t)\}$, with $A_1(t) = 2a_1^2(t)$ and $A_2(t) = 2a_2^2(t)$, gives the corresponding momenta. The Hamiltonian of the system is expressed as

$$H = -L + \int_{-\infty}^{\infty} \frac{i}{2} \left(\frac{\partial \psi}{\partial t} \psi^* - \frac{\partial \psi^*}{\partial t} \psi \right) dx. \quad (12)$$

Considering the integration limits imposed by the new

geometry, we have

$$\begin{aligned}
H = \pi \Big\{ & A_0^2 [2k^2 + V_0 + A_0^2 s(t)] + \frac{s(t)}{4} (A_1^2 + A_2^2) \\
& + A_1 \left[(k+q)^2 + \frac{V_0}{2} - A_0^2 q^2 \eta(t) + 2A_0^2 s(t) \right] \\
& + A_2 \left[(k-q)^2 + \frac{V_0}{2} - A_0^2 q^2 \eta(t) + 2A_0^2 s(t) \right] \\
& + \sqrt{A_1} \sqrt{A_2} s(t) \left[2A_0^2 \cos(b_1 + b_2) + \sqrt{A_1} \sqrt{A_2} \right] \\
& - \sqrt{A_1} \sqrt{A_2} q^2 \eta(t) \left[2A_0^2 \cos(b_1 + b_2) + \sqrt{A_1} \sqrt{A_2} \right] \Big\}, \quad (13)
\end{aligned}$$

In order to derive the evolution equations for the time-dependent parameters introduced in Eq. (10), we use the corresponding Euler-Lagrange equations based on the variational effective Lagrangian L_{eff} . In the generalized form, these equations read

$$\frac{d}{dt} \left(\frac{\partial L_{\text{eff}}}{\partial \dot{\xi}_i} \right) - \frac{\partial L_{\text{eff}}}{\partial \xi_i} = 0, \quad (14)$$

where ξ_i and $\dot{\xi}_i$ are, respectively, the generalized coordinate and corresponding generalized momentum. Hence, the evolution equation corresponding to the variational parameter a_1 is

$$\frac{\partial a_1}{\partial t} = (q^2 \eta(t) - s(t)) A_0^2 a_2 \sin(b_1 + b_2). \quad (15)$$

For the parameter b_1 the evolution equation reads

$$\begin{aligned}
\frac{\partial b_1}{\partial t} = & -2kq - q^2 - \frac{V_0}{2} - s(t) (A_0^2 + a_1^2 + 2a_2^2) + q^2 \eta(t) \\
& \times (A_0^2 + 4a_2^2) + (q^2 \eta(t) - s(t)) A_0^2 \frac{a_2}{a_1} \cos(b_1 + b_2). \quad (16)
\end{aligned}$$

For the parameter a_2 , we get

$$\frac{\partial a_2}{\partial t} = (q^2 \eta(t) - s(t)) A_0^2 a_1 \sin(b_1 + b_2), \quad (17)$$

and for the parameter b_2 , the evolution equation is

$$\begin{aligned}
\frac{\partial b_2}{\partial t} = & 2kq - q^2 - \frac{V_0}{2} - s(t) (A_0^2 + 2a_1^2 + a_2^2) + q^2 \eta(t) \\
& \times (A_0^2 + 4a_1^2) + (q^2 \eta(t) - s(t)) A_0^2 \frac{a_1}{a_2} \cos(b_1 + b_2). \quad (18)
\end{aligned}$$

For simplicity, we may use a variant of the ansatz (10) for which

$$a_1 = a_2 = a, \quad \text{and} \quad b_1 + b_2 = b. \quad (19)$$

Then the coupled ordinary differential equations for $a(t)$ and $b(t)$ are

$$\frac{\partial a}{\partial t} = (q^2 \eta(t) - s(t)) A_0^2 a \sin(b), \quad (20)$$

and

$$\begin{aligned}
\frac{\partial b}{\partial t} = & -2q^2 - V_0 + 2q^2 \eta(t) (A_0^2 + 4a^2) - 2s(t) (A_0^2 + 3a^2) \\
& + 2(q^2 \eta(t) - s(t)) A_0^2 \cos(b). \quad (21)
\end{aligned}$$

Using Eq. (19), we rewrite the Hamiltonian of the system given by Eq. (13) into a more simple form as

$$\begin{aligned}
H = \pi \Big\{ & A_0^2 (2k^2 + V_0 + A_0^2 s(t)) \\
& + A [2(k^2 + q^2 - q^2 (A_0^2 - A) \eta(t)) + V_0] \\
& + A \left(4A_0^2 + \frac{3}{2} A \right) s(t) + 2A_0^2 A \cos(b) (s(t) - q^2 \eta(t)) \Big\}. \quad (22)
\end{aligned}$$

However, we have found that $A(t)$ and $b(t)$ are canonically conjugate with respect to an effective Hamiltonian H_{eff} (i.e. $\frac{\partial A}{\partial t} = -\frac{\partial H_{\text{eff}}}{\partial b}$ and $\frac{\partial b}{\partial t} = \frac{\partial H_{\text{eff}}}{\partial A}$) which reads

$$\begin{aligned}
H_{\text{eff}}(A) = & - \left[V_0 A + 2q^2 A + \frac{3}{2} s(t) A^2 + 2s(t) A_0^2 A \right. \\
& - 2q^2 \eta(t) (A_0^2 + A) A + 2(s(t) \\
& \left. - q^2 \eta(t)) A_0^2 A \cos(b) \right]. \quad (23)
\end{aligned}$$

In the absence of lattice, this effective Hamiltonian is an exact integral of motion on the subspace spanned by the ansatz (10). Using $A(t=0) = 0$ (without loss of generality) in Eq. (23) yields $H_{\text{eff}}^0 = H_{\text{eff}}(A(t=0)) = 0$. Since the Hamiltonian is not conserved in the presence of OL, the non-conservative part of the Hamiltonian may transfer an energy, say E_{com} , to the center of mass of the solitons eventually generated in the case of MI. Thus we may write $H_{\text{eff}}^0 - E_{\text{com}} = H_{\text{eff}}(A)$ and then obtain

$$\begin{aligned}
& V_0 A + 2q^2 A + \frac{3}{2} A^2 s(t) + 2A_0^2 A s(t) \\
& - 2Aq^2 \eta(t) (A_0^2 + A) + 2A_0^2 A \cos(b) (s(t) - q^2 \eta(t)) = E_{\text{com}}. \quad (24)
\end{aligned}$$

One may easily rewrite Eq. (20) in terms of the generalized momentum A . Then eliminating the generalized coordinate b between the resultant equation and Eq. (24), we come to the following energy equation for A :

$$\frac{1}{2} \dot{A}^2 + V_{\text{eff}} = 0, \quad (25)$$

where the effective potential reads

$$\begin{aligned}
V_{\text{eff}} = & 2A^2 q^2 [q^2 + 2s(t) A_0^2 - 2A_0^2 q^2 \eta(t)] \\
& + 2A^2 V_0 (q^2 + \frac{V_0}{4} + s(t) A_0^2 - A_0^2 q^2 \eta(t)) \\
& + A^3 [3s(t) (q^2 + \frac{V_0}{2} + A_0^2 s(t))] \quad (26) \\
& + A^3 [q^2 \eta(t) (4A_0^2 q^2 \eta(t) - 7A_0^2 s(t) - 4q^2 - 2V_0)] \\
& + A^4 [q^2 \eta(t) (2q^2 \eta(t) - 3s(t)) + \frac{9}{8} s(t)^2] + V_{\text{eff}}^0.
\end{aligned}$$

The coefficient V_{eff}^0 depends on E_{com} , V_s , g and σ .

Through the effective potential in Eq. (26), we can find the information about the dynamical properties of the system. For instance, the evaluation of the curvature of the potential at $A = 0$ may determine whether the dynamics is stable or not. When the potential is concave, i.e., the second derivative $\frac{\partial^2 V_{\text{eff}}}{\partial A^2}|_{A=0}$ is negative, the dynamics is unstable. Otherwise when $\frac{\partial^2 V_{\text{eff}}}{\partial A^2}|_{A=0}$ is positive, the potential is convex and the dynamics is stable. We take advantage of such mathematical evidence to find the MI criteria of the system. Hence for the dynamics to be unstable, we should have $\frac{\partial^2 V_{\text{eff}}}{\partial A^2}|_{A=0} = 4[q^2(q^2 + 2s(t)A_0^2 + V_0 - 2A_0^2q^2\eta(t))] + 4V_0[(\frac{V_0}{4} + s(t)A_0^2 - A_0^2q^2\eta(t))] + v_0$ negative. For a safe domain of parameters, the coefficient $v_0 = \frac{\partial^2 V_{\text{eff}}}{\partial A^2}|_{A=0}$ is small and then can be neglected [56]. In such a domain, the condition for exciting the MI reads

$$V_0^2 + 4(q^2 + gl(t)A_0^2 - \sigma gl(t)^{-1}q^2A_0^2)V_0 + 4q^2(q^2 + 2gl(t)A_0^2 - 2\sigma gl(t)^{-1}q^2A_0^2) < 0. \quad (27)$$

To study the instability of the system with respect to the initial parameters α , V_s , g and g_2 , we may rewrite Eq. (27) as

$$V_s^2 + 4[Q(t)^2 + S(t)A_0^2 - \sigma S(t)Q(t)^2A_0^2]V_s + 4Q(t)^2[Q(t)^2 + 2S(t)A_0^2 - 2\sigma S(t)Q(t)^2A_0^2] < 0, \quad (28)$$

where $Q(t) = q(1 + 4\alpha t^2)^{\frac{1}{2}}$ and $S(t) = g(1 + 4\alpha t^2)^{\frac{1}{2}}$, i.e. $Q(t) = ql(t)^{-1}$ and $S(t) = gl(t)^{-1}$. At the initial time (or in the absence of harmonic trap), we readily have $Q = q$, $S = g$, and $V_s = V_0$, and then Eqs. (27) and (28) are equivalent. Eq. (28) is a time-dependent criterion that defines the occurrence of MI in BECs with OL and shape-dependent confinement potential for an atom evolving within the condensates. In a similar way, Eqs. (20) and (21) may be rewritten as follows:

$$\begin{aligned} \frac{\partial a}{\partial t} &= -gl^{-1}(1 - \sigma Q^2)A_0^2a \sin(b), \\ \frac{\partial b}{\partial t} &= -2Q^2 - V_s - 2gl^{-1}(1 - \sigma Q^2)A_0^2 \\ &\quad - 2gl^{-1}(3 - 4\sigma Q^2)a^2 - 2gl^{-1}(1 - \sigma Q^2)A_0^2 \cos(b). \end{aligned} \quad (29)$$

In Eq. (29) especially, Q and l are functions of t which is the time in the original dimensionless Eq. (5).

Using the conditions in Eqs. (27) and (28), we can find a lot of information on the dynamical instability of the system with respect to the internal properties of the condensate, the external perturbation and the external trapping characteristics. Actually they relate in a very simple way the confinement strength α of harmonic potential, the strength V_s of optical potential, the two-body contact interaction term g , the two-body interaction correction term σ due to shape-dependent confinement, and

the perturbation wave number q . From Eq. (28), the local growth rate of instability can be obtained. It is given by the relation

$$\text{Gain} = \left[- \left(V_s^2 + 4(Q^2 + SA_0^2 - \sigma SQ^2A_0^2)V_s + 4Q^2(Q^2 + 2SA_0^2 - 2\sigma SQ^2A_0^2) \right) \right]^{1/2}. \quad (30)$$

In the particular case where the BEC is not immersed in an OL potential, that is, $V_s = 0$, we readily obtain from Eq. (27) that $q^2 + 2gA_0^2(1 + 4\alpha t^2)^{-\frac{1}{2}} - 2A_0^2q^2gg_2(1 + 4\alpha t^2)^{\frac{1}{2}} < 0$, which is exactly the same instability condition as discussed in Ref. [60]. A similar condition can also be obtained from Ref. [55]. Moreover, in the absence of the HOI and OL potential, i.e. $\sigma = V_s = 0$, we have $q^2 < -2gA_0^2(1 + 4\alpha t^2)^{-\frac{1}{2}}$, which is the instability condition obtained in a previous study of MI through the NLS equation with focusing nonlinearity and quadratic potential [38]. From the condition in Eq. (28), one can obtain that the instability diagram in the q - V_s plane, for both attractive and repulsive two-body interactions, has at least three regions bounded by two parabolic lines defined by $V_s = -2l(t)^{-2}q^2$ and $V_s = -2l(t)^{-2}(1 - \sigma l(t)^{-1}/\sigma_c)q^2 - 4gA_0^2l(t)^{-1}$, with $\sigma_c = 1/(2gA_0^2)$.

In what follows, we check in detail the dynamical instability of the system in both cases of attractive and repulsive two-body interactions. In calculations, we use $\alpha = 0.00633$, $A_0 = 1.0$, and $q = 0.5$, if not explicitly stated. To obtain the evolution of the perturbation, we will numerically solve Eq. (29), with initial conditions $a(0) = 0.01$ and $b(0) = 0.01$, through a fourth-order Runge-Kutta scheme. All quantities plotted are dimensionless.

B. Dynamical instability in the case of two-body repulsion

From previous works, we know that dynamical instability does not arise in a condensate with repulsive two-body interactions ($g > 0$) whatever the excitation wave number is. Here, we predict that the dynamical instability of a BEC with two-body attraction can drastically change in the presence of both the OL and the HOI. In Fig. 1, we display the instability diagrams of the system as a function of the OL strength V_s and wave number q of the excitations for different values of the strength of HOI, σ , when the two-body interaction in the condensate is repulsive ($g = +1$). To plot panels (A) and (B), we computed the instability growth rate of the system at time $t = 0$. For panels (C) and (D), the color scale indicates the maximum over time of the instability growth rate of the system for runs up to $t = 9.0$, which is close to the analytical limiting time $\pi/(4\sqrt{\alpha})$. Similar pictures may be obtained by computing the integrated gain instead of the maximal gain over the same time interval. The dark blue regions of each panel depict

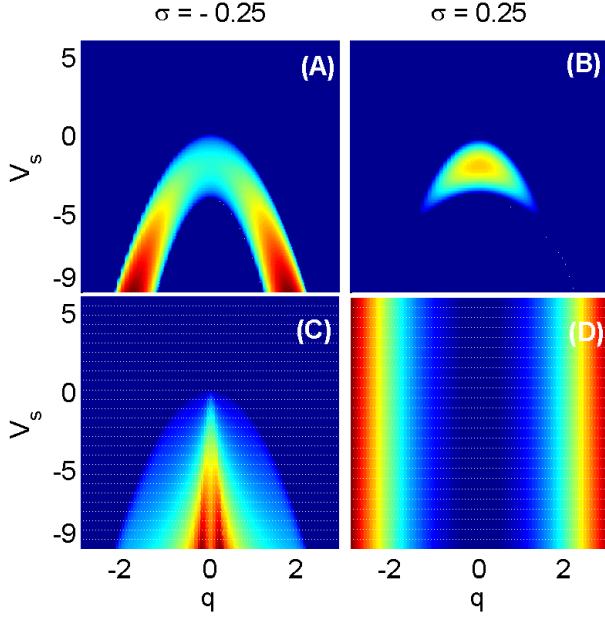


FIG. 1: Instability diagrams as a function of the OL strength V_s and wave number q of the excitations, for different values of the HOI parameter σ when the two-body interaction is repulsive ($g = +1$). The dark blue and light colored regions correspond to the modes for which the system is modulationally stable and unstable, respectively. The color scale in panels (A) and (B) indicates the growth rate of the unstable modes at time $t = 0$ for a given (q, V_s) . In panels (C) and (D), the color scale indicates the maximum growth rate of the unstable modes over time for a given (q, V_s) . The time runs up to $t = 9.0$, very close to the singularity time $\pi/(4\sqrt{\alpha})$ and enough to allow observing dynamical instability in our system.

stable modes while the rest of the domain corresponds to unstable modes. The shapes of the initial and all-time instability diagrams displayed in left panels (A) and (C), respectively, are common for any negative value of the parameter σ . Besides, while the all-time instability diagram given in panel (D) is common for all positive σ , the shape of the initial instability diagram as displayed in panel (B) may differ depending whether $\sigma < \sigma_c$, $\sigma = \sigma_c$ or $\sigma > \sigma_c$, with $\sigma_c = 1/(2gA_0^2)$ (positive). The dynamical instability of the BECs with two-body interactions is strongly determined by the sign of the HOI parameter.

First, we consider the case where $\sigma > 0$. From Figs. 1(B) and (D), we infer that all modes in the q - V_s plane may eventually lead to dynamical instability. Moreover at longer times, the instability growth rate in the system may be almost independent of the OL strength as we have vertical lines in the color scale in panel (D). Short-wavelength excitations (with big wave numbers) are completely unstable while long-wavelength excitations (with small wave numbers) may be stable for a short time when the perturbation begins. The occurrence of instability in the system is seriously affected by

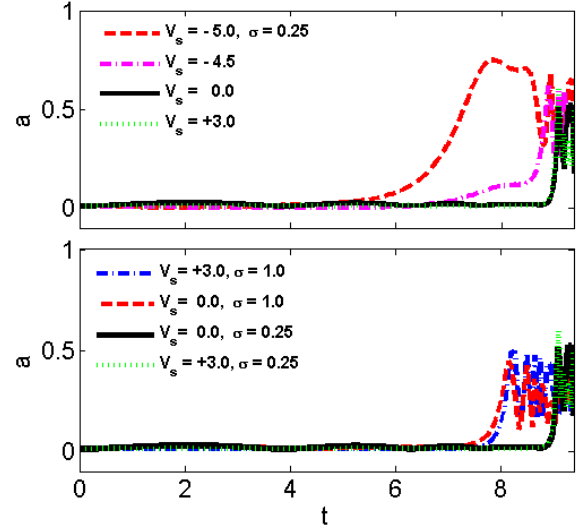


FIG. 2: The time evolution of the modulational perturbation a , described by Eq. (29), for different strengths of the OL potential, when the HOI parameter is positive and the two-body interaction repulsive ($g = +1$). The initial condition used in the computation is $a(0) = 0.01$. In the top panel, $\sigma = 0.25$. The wave number q is modulationally unstable (exponential growth) for all OL strengths. In the bottom panel, we plot the comparative evolution of the perturbation for two values of the HOI parameter, namely $\sigma = 0.25$ and 1.0 , and for various values of the OL strength. For each value of σ , the curves for $V_s = 0.0$ and $V_s = 3.0$ are almost merged, and then correspond to the same instability onset time.

the OL strength only for $V_s \leq -4gA_0^2$. Meanwhile, the occurrence of instability is strongly affected by the HOI parameter. Increasing the parameter σ enhances the instability in the system, and it occurs earlier. That behavior can be clearly justified through the theoretical time evolution of the perturbation amplitude in the system. For this, we numerically solve Eq. (29), with initial conditions $a(0) = 0.01$ and $b(0) = 0.01$. The corresponding evolution of the perturbation amplitude in the system is displayed in Fig. 2. The amplitude of the excitations exponentially grows for all values of the OL parameter, showing the instability of the system. In the top panel, for same strength of HOI ($\sigma = 0.25$) the instability onset time ($t \approx 9.1$) is almost identical for $V_s = 0.0$ and 3.0 , all greater than $-4.0 \equiv -4gA_0^2$. The instability onset time changes with the OL parameter for $V_s = -4.5$, $-5.0 \leq -4.0$; it is, respectively, $t \approx 8.9$ and $t \approx 7.8$, and so increases with $|V_s|$. In the bottom panel, the exponential growth arises around $t = 9.1$ for $\sigma = 0.25$, and $t = 8.1$ for $\sigma = 1.0$ in any of the relevant modes. Then for a bigger strength of HOI, the instability onset time shortens, showing that the system becomes more unstable. Thus the repulsive HOI ($\sigma > 0$) is expected to be destabilizing for a BEC with two-body repulsion. In such a condensate, the OL strength enhances the dynamical instability for $V_s \leq -4gA_0^2$, and does not affect it for

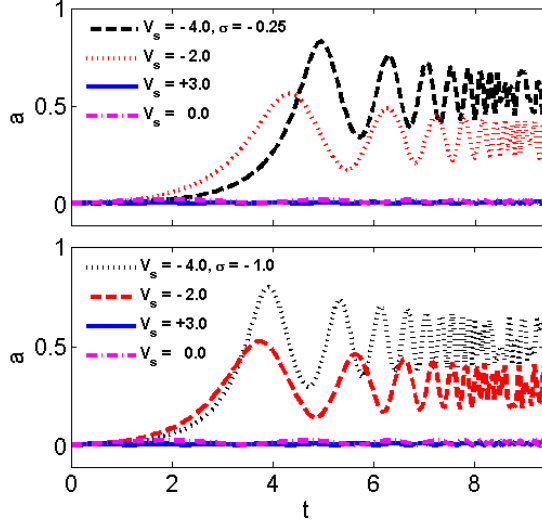


FIG. 3: The modulatory perturbation a as a function of time for different strengths of the OL potential, when the HOI parameter is negative and the two-body interaction repulsive ($g = +1$). The plots are obtained by solving Eq. (29) with the initial condition $a(0) = 0.01$. In the top and bottom panels, $\sigma = -0.25, -1.0$, respectively. Both panels show that the excitation is modulationally unstable (exponential growth) for OL strengths $V_s = -4.0, -2.0$, and stable for $V_s = 0.0, +3.0$. Note that the curves for $V_s = 0.0$ and 3.0 are merged in the displayed time scale.

$$V_s > -4gA_0^2.$$

Secondly, we consider the case where $\sigma \leq 0$. From Figs. 1(A) and (C), we infer that not all modes may undergo dynamical instability. The parameter domain in the q - V_s plane has two main regions bounded by the line $V_s = -2q^2$. Any excitation with wave number q is expected to be stable for OL strengths $V_s > -2q^2$, and unstable for OL strengths $V_s < -2q^2$. In other words, for $V_s \geq 0$ all excitations are stable. For $V_s < 0$ long-wavelength excitations defined by $q^2 < \sqrt{-V_s}/2$ are unstable while short-wavelength excitations ($q^2 > \sqrt{-V_s}/2$) are stable. Within the unstable domain, the system may become more unstable as the HOI strengthens. We realized that in such a domain, the instability gain increases with $|\sigma|$. The unstable bandwidth in the wave number spectrum enlarges and then more modes become unstable. We display in Fig. 3 the theoretical time evolution of the modulatory perturbation to make it clear. In both panels, the excitation amplitude for the modes with OL strength $V_s = 0.0$ and $+3.0$, both greater than $-0.50 \equiv -2q^2$, oscillates in time around its initial value $a(0) = 0.01$, which means that the system is dynamically stable. The excitation amplitude for the modes with OL strength $V_s = -4.0$ and -2.0 , all less than $-2q^2$, exponentially grows in time. Moreover, in the bottom panel for instance, with the same strength of HOI ($\sigma = -1.0$), the onset of instability for the unstable OL strengths is different, notably $t \approx 2.7$ and 3.2 corre-

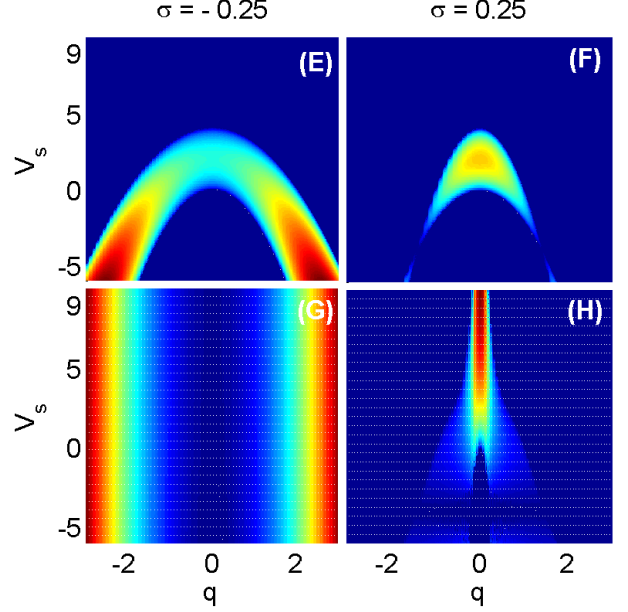


FIG. 4: Instability diagrams as a function of the OL strength V_s and wave number q of the excitations, for different values of the HOI parameter σ when the two-body interaction is attractive. The dark blue and light colored regions correspond to the modes for which the system is modulationally stable and unstable, respectively. The color scale indicates the growth rate of the unstable modes for a given (q, V_s) . The color scale in panels (E) and (F) indicates the growth rate of the unstable modes at time $t = 0$ for a given (q, V_s) . In panels (G) and (H), the color scale indicates the maximum growth rate of the unstable modes over time (for runs up to $t = 9.0$) for a given (q, V_s) .

sponding to $V_s = -4.0$ and -2.0 , respectively. As we can see from both panels of Fig. 3, with the same strength of OL, the onset of instability for different unstable HOI strengths is not the same. Notably with $V_s = -4.0$, we get $t \approx 4.9$ (top panel) and 3.9 (bottom panel) corresponding to $\sigma = -0.25$ and -1.0 , respectively. Thus, for a bigger strength of HOI (in modulus), the instability onset time shortens, showing that the system becomes more unstable. Hence, the occurrence of instability in a condensate with two-body repulsion depends on the values of the HOI and OL strengths. Increasing $|\sigma|$ and/or V_s shortens the onset time of the exponential growth and then enhances the instability in the system with negative HOI parameter. As shown above, almost similar results are obtained in the case where the HOI parameter is positive. With two-body repulsion in the condensate, the possibility to get modulational stability occurs when $\sigma \leq 0$ and $V_s > -2q^2$, with q being the wave number of the excitation.

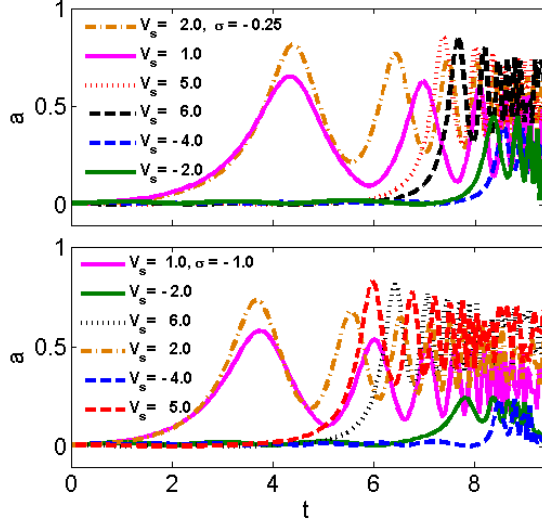


FIG. 5: The evolution of the modulational perturbation a as a function of time for different strengths of the OL potential, when the HOI parameter is negative and the two-body interaction attractive ($g = -1$). The plots are obtained by solving Eq. (29) with the initial condition $a(0) = 0.01$. The wave number q is modulationally unstable (exponential growth) for all OL strengths when the HOI parameter is negative. In the top and bottom panels, the HOI parameter is $\sigma = -0.25$ and -1.0 , respectively.

C. Dynamical instability in the case of two-body attraction

Dynamical instability generally arises in a condensate with attractive two-body interactions ($g < 0$) in a wide range of wave numbers. In this section, we predict that such a behavior may be deeply modified in the presence of OL and HOI. To this end, we portray in Fig. 4 the instability diagrams of the system as a function of the OL strength and wave number q of the excitations for different values of the strength of HOI in the case where the two-body interaction in the condensate is attractive ($g = -1$). We obtained panels (E) and (F) by computing the instability growth rate at time $t = 0$, and panels (G) and (H) by computing the maximum instability gain over time for runs up to 9.0, close to the limiting time $\pi/(4\sqrt{\alpha})$. The dark blue regions of the panels may be stable while the rest of the domain is unstable. The shapes of the initial and all-time instability diagrams displayed in right panels (F) and (H), respectively, are common for any positive value of σ . Besides, while the all-time instability diagram given in panel (G) is common for all positive σ , the shape of the initial instability diagram as displayed in panel (E) may differ depending whether $\sigma < \sigma_c$, $\sigma = \sigma_c$ or $\sigma > \sigma_c$, with $\sigma_c = 1/(2gA_0^2)$ (negative). Similarly to the previous section, we study the dynamical instability of the BECs with two-body repulsion in two different regimes of the HOI parameter.

We start with the first regime, where $\sigma < 0$. From

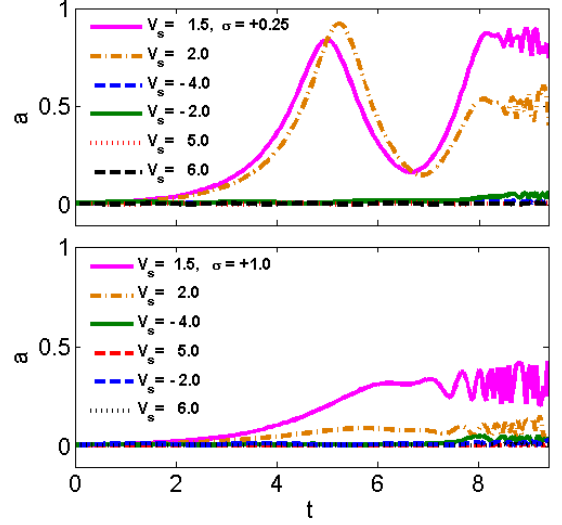


FIG. 6: The evolution of the modulational perturbation a as a function of time for different strengths of the OL potential, when the HOI parameter is positive and the two-body interaction attractive ($g = -1$). The plots are obtained by solving Eq. (29) with the initial condition $a(0) = 0.01$. In the upper and lower panels, $\sigma = 0.25$ and 1.0 , respectively. In the upper panel, all modes undergo exponential growth from the initial amplitude. In the lower panel (where the HOI strength is higher), the plots for the modes with $V_s = -4.0, -2.0, 5.0$ and 6.0 , almost merged, depict stable oscillations around the initial amplitude. These modes are all situated in the two initially stable regions in Fig. 4(F). However, we realized that only the modes with $V_s = 5.0$ and 6.0 can keep oscillating at longer times. The modes with $V_s = -4.0$ and -2.0 later develop exponential growth.

Figs. 4(E) and (G), we infer that all modes may be dynamically unstable in the relevant time scale as seen in panel (G). Moreover at longer times, the instability growth rate is independent of the OL strength as we have vertical lines in the color scale in that panel. Short-wavelength excitations are unstable, especially those that lie in the initially unstable domain while long-wavelength excitations may be stable but for limited times. In particular, the long-wavelength excitations that lie in the initially unstable domain, i.e., the light green region in the middle of the instability diagram in panel (E), are readily unstable. This suggests that the occurrence of instability is affected by the OL strength. Meanwhile, the HOI parameter strongly affects the onset of instability in the system as well. Increasing $|\sigma|$ enhances the instability in the system. That feature can be clearly checked through the theoretical time evolution of the perturbation amplitude in the system. The corresponding evolution of the perturbation amplitude in the system is displayed in Fig. 5. For calculations, we used $\alpha = 0.00633$ and $q = 0.5$. The amplitude of the excitation exponentially grows for all values of the OL parameter. In the top panel, for same strength of HOI ($\sigma = -0.25$), the instability onset time is different

for $V_s = -4.0, -2.0, V_s = 1.0, 2.0$, and $V_s = 5.0, 6.0$, respectively, picked from the bottom, middle and top parts of the instability diagram in Fig. 4(E). The instability onset times depend on both the OL and HOI parameters. As we can see in the upper panel of Fig. 5, the instability onset time increases in the order $V_s = 1.0, 2.0, 5.0, 6.0$, and $V_s = -2.0, -4.0$. Hence, the instability begins with the modes in the middle region (initially unstable), then spreads to the modes in the top region (initially stable), before reaching the modes in the bottom region (initially stable) depicted in Fig. 4(E). Within the same region, the instability onset time weakly increases and the instability gain slightly decreases when $|V_s|$ increases, except for the modes in the middle region. Thus increasing the OL strength softens the instability in the system for most of the modes. Comparing the upper and lower panels of Fig. 5, it emerges that the instability onset time shortens when $|\sigma|$ increases. So the attractive HOI (negative σ) is destabilizing for a condensate with two-body attraction, while the OL slightly softens the instability for initially stable modes and enhances it for initially unstable modes.

Now let us consider the second regime, where $\sigma \geq 0$. From Figs. 4(F) and (H), we infer that not all modes may be dynamically unstable. The parameter domain in the q - V_s plane has two main regions as depicted in panel (H). The modes in the middle region are unstable while the rest of the domain (dark blue region) may be stable. Most excitations with wave number q are expected to be stable for OL strengths $V_s > -4gA_0^2$. However, some modes satisfying that condition, and having very small wave number can remain unstable. For $-4gA_0^2 > V_s > -2/\sigma$, long-wavelength excitations defined by $q^2 < \frac{-V_s - 4gA_0^2}{2(1 - 2gA_0^2)}$ are unstable while short-wavelength excitations with $q^2 > \frac{-V_s - 4gA_0^2}{2(1 - 2gA_0^2)}$ may be stable. For $V_s < -2/\sigma$, almost all excitations may be unstable. Within the unstable domain, the system may become less unstable as the HOI strengthens. We display in Fig. 6 the theoretical time evolution of the modulational perturbation to clarify that behavior. In both panels, the excitation amplitude for the modes with OL strengths $V_s = 1.5$ and 2.0 readily undergo exponential growth in time. The growth onset is delayed in other modes. Hence, considering the instability diagram in Fig. 4(F), the instability arises earlier in the modes from the initially unstable region, later in the lower region and very late in the upper region. Thus the range where the OL strength is chosen seriously affects the stability of the condensate. Comparing both panels of Fig. 6, we obtain that the repulsive HOI (positive σ) is stabilizing for a condensate. In fact, the instability onset is delayed and the instability gain reduced in all unstable modes when the HOI strength is increased from $\sigma = 0.25$ (upper panel) to $\sigma = 1.0$ (lower panel). For instance, considering the mode with $V_s = 1.5$, we obtain the instability onset times $t \approx 5.0$ (in the upper panel where $\max(a) \approx 0.9$) and $t \approx 6.0$ (in the lower panel where $\max(a) \approx 0.4 < 0.9$). Moreover, some unstable modes in the upper panel defined by $V_s > 4.0 \equiv -4gA_0^2$ may even

become stable in the lower panel. However, this stability ends at larger times which increase with the value of σ .

Hence, the occurrence of instability in a condensate with two-body attraction depends on the values of the HOI and OL strengths. Increasing σ enlarges the onset time of the exponential growth and then softens the instability in the system with positive HOI parameter. This is in contradiction with the case above where the HOI parameter is negative. In such case, as we have previously seen, increasing $|\sigma|$ rather reduces the onset time of the exponential growth and then enhances the instability in the system. Meanwhile, increasing V_s delays the exponential growth and then softens the instability in the system with positive as well as negative HOI parameter, except for initially unstable modes where it rather enhances the instability. With two-body attraction in the condensate, the possibility to get dynamical stability arises when $\sigma > 0$ and $V_s > -4gA_0^2$, with q being the wave number of the excitation. As noted above, the effective occurrence of this stability requires, in particular, the systems with sufficiently large values of the HOI parameter σ . Moreover, this dynamical stability may vanish at larger times.

IV. DIRECT NUMERICAL ANALYSIS

The above analytical results give predictions of the instability onset in the system. However they are based on the linear stability analysis of an unperturbed carrier wave. The validity of such an analysis is limited to amplitudes of perturbation small in comparison with that of the carrier wave. Moreover, because of the useful analytical methods, the accessible times are limited to $\frac{\pi}{4\sqrt{\alpha}} \approx 9.9$ for $\alpha = 0.00633$ as used in most calculations. Analytical calculations therefore cannot tell us, neither the evolution of strongly perturbed wave nor, the long-time evolution of a modulated extended nonlinear wave. In order to check the validity of our predictions and go beyond the limiting time and linearization, we perform direct numerical integrations of the full GP Eq. (5). We used the following initial configuration [57, 58],

$$\psi(x, 0) = \psi_{\text{TF}}[\phi_0 + \varepsilon \cos(qx)], \quad (31)$$

where $\psi_{\text{TF}} = \sqrt{\max[0, \mu - V(x)]}$ is the background wave function in the Thomas-Fermi approximation, with $V(x) = \alpha x^2 + 0.5 \cos(x)^2$. The chemical potential $\mu = 1$ and the strength of magnetic field $\alpha = 1/(4\pi)^2 \approx 0.00633$ are used in all numerical calculations. We have taken $\varepsilon = 0.01$, which is sufficiently small and will not cause significant variation in the qualitative nature of the results. The initial amplitude $\phi_0 \equiv A_0 = 1.0$ is used in all computations. The boundary condition is periodic, and due to that we let $q = n\pi\sqrt{\alpha}$. In what follows, we choose $n = 2$ to investigate the effect of both the HOI and the OL in the dynamics of the corresponding (long-wavelength) excitation. Following the same spirit as in

the analytical part, we consider separately the cases of two-body repulsion and attraction.

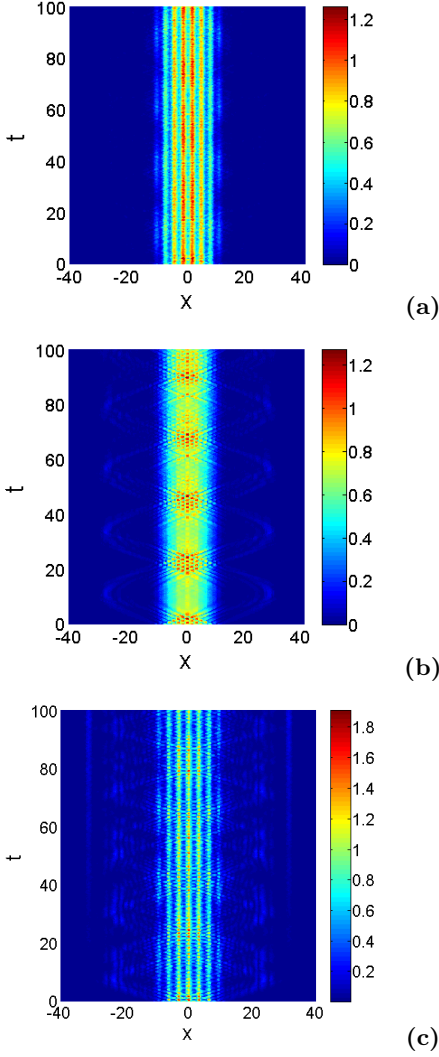


FIG. 7: Numerical space-time evolution of the wave in the system with two-body repulsion and attractive HOI for runs up to $t = 100$, and for $g = 1.0$, $\sigma = -0.25$, and (a) $V_s = 3.0$, (b) $V_s = -0.25$, (c) $V_s = -4.0$. Mild oscillations in panels (a) and (b) show that the system is dynamically stable. Panel (c) displays the oscillatory instability of the system. We note in passing that we obtained a plot very similar to panel (b) with same parameters except for $V_s = 0.0$ (absence of OL).

We begin by launching numerical calculations for the case of BECs, with *repulsive* two-body interactions ($g = +1$), trapped in both harmonic and optical fields. As is known from previous works, such a condensate is dynamically stable for any wave number in the absence of OL and HOI. Here, we switch on the optical potential, and check what happens to the stability of the system.

Fig. 7 portrays the 3D evolution of the square amplitude of the wave in the system in time and space for negative HOI parameter ($\sigma \leq 0$). Panels (a) and (b) correspond to the case where the parameters are picked in the

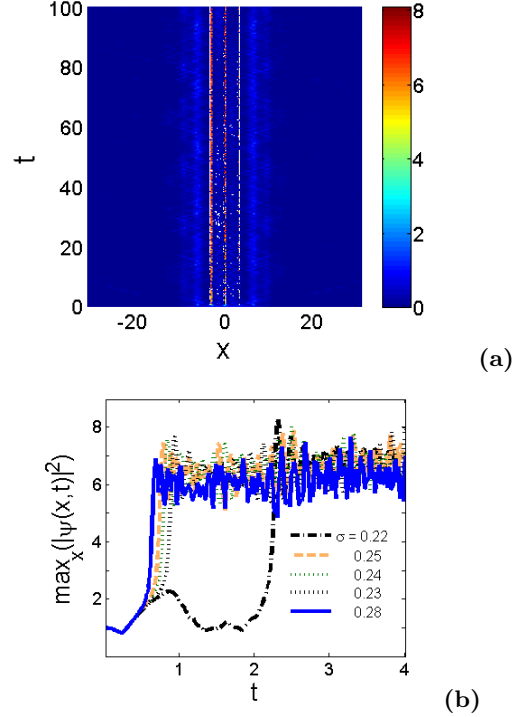


FIG. 8: Numerical dynamics of the wave in the system with two-body repulsion and repulsive HOI ($\sigma > 0$) for runs up to $t = 100$, and for $g = 1.0$ and $V_s > -4.0$. Panel (a) shows the unstable space-time evolution of the wave for $\sigma = +0.25$ and $V_s = -2.0$. Panel (b) depicts the comparative evolution of the wave amplitudes for $V_s = -2.0$ and for $\sigma = +0.22$, $+0.23$, $+0.25$, $+0.28$. We display the time evolution only up to $t = 4.0$ to make visible the separation between the curves, and then the MI onset times.

domain predicted to be stable, i.e., $V_s > -0.5 \equiv -2q^2$. The difference between both panels is that in (a) the OL strength is positive and in (b), it is negative ($0 \geq V_s > -0.5$). It should be noted that the case where the OL is switched off belongs to that range. Panel (c) corresponds to the case predicted to be unstable. The plot in Fig. 7(a) shows that the wave amplitude exhibits mild oscillations both in time and space around its initial value. Actually the amplitude can go from 1.0 to roughly 1.1 only. The shape as well as density of the condensate are preserved in time and space. The breathing behavior demonstrates that the system is completely stable indeed. In Fig. 7(b) the wave is split into three components. Two very tiny fractions of the condensate perform regular oscillations in opposite directions with same frequency and spatial amplitude that goes beyond the OL. The main fraction exhibits mild oscillations in time as well and the shape of the condensate is almost preserved in time and space, demonstrating the stability of the system. However, in contradiction to the case of panel (a), the distribution of condensed atoms in the OL wells is not clearly seen, and a negligible fraction of the condensate can regularly oscillate in space and time. We suggest that these obser-

variations, which do not alter the stability of the system, are due to the low height of the interwell barrier of the OL. The role played by the OL in this stability is not negligible. In fact, for the same parameters except for $V_s = -4.0$, the system becomes unstable. We observed the same behavior for $V_s = -3.0 < -0.5$. However, the corresponding instability is oscillatory, as displayed in Fig. 7(c). The system undergoes irregular oscillations with higher amplitudes both in time and space. The maximum square amplitude increases to roughly 1.9, which is bigger than 1.3 obtained in panels (a) and (b) but not big enough as in usual MI. So we may say that a slight growth rather than a clear exponential growth is observed in the wave amplitude. The instability manifests itself not through serious localization, but in the form of scattering of the wave envelope in space, which is its salient feature. The many fractions of condensate resulting from the scattering perform complex oscillations in space and time. In particular, the condensate fractions loaded in the outer region of the trap are the most sensitive to oscillatory instability. In our context, the sign of the OL strength induces indeed a small change in the trapping configuration. A positive OL strength causes the magnetic trap (MT) center to coincide with a well of the OL, while a negative OL strength causes the MT center to coincide with an interwell barrier. Hence trapped BECs with repulsive two-body interactions and attractive HOI, in the presence of excitations of wave number q and OL of strength V_s , exhibit oscillatory instability for $V_s < -2q^2$, i.e., when a high OL interwell barrier exists in the center of the magnetic trap. This instability, typically induced by OLs, is characterized by a spatial scattering of the wave. Such BECs rather exhibit dynamical stability for $V_s > -2q^2$, i.e., when an OL well or a low OL interwell barrier exists in the MT center. This stability preserves the height and width of the initial wave.

Let us examine the case of BECs with repulsive two-body interactions but in the presence of repulsive HOI. When $V_s < -4.0 \equiv -4gA_0^2$, the dynamical behavior of the system is similar to the one plotted in Fig. 7(c). So the BEC undergoes oscillatory instability. When $V_s > -4.0$, we show in Fig. 8 (a) the 3D space-time evolution of the wave in the case of positive HOI parameter predicted to be unstable. We realize that an exponential growth arises in the amplitude of the wave due to the perturbation. The square amplitude can quickly increase from 1.0 to 8.0, which means that the system is dynamically unstable. The inner region of the MT is more affected by dynamical instability than the outer region. However, as we observed, the instability expands to OL wells in the outer region of the MT as the OL strength (or the HOI) increases. Thus, in both cases $V_s < -4.0$ and $V_s > -4.0$, the system is unstable. The instability is oscillatory for $V_s < -4gA_0^2$ and dynamical for $V_s > -4gA_0^2$. In the dynamically unstable parameter domain, the OL strength causes the instability to expand from the MT center to the outer region of the MT. Fig. 8 (b) displays the effect of the HOI in the onset of dynamical

instability of the condensate. The OL strength is chosen in the dynamically unstable domain. The onset time of the exponential growth shortens when the HOI parameter increases, and the system becomes more unstable. Thus the positive HOI parameter clearly appears to be destabilizing for repulsive BECs.

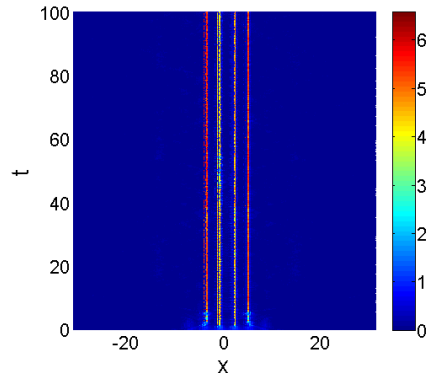


FIG. 9: Numerical dynamics of the wave in the system with two-body attraction ($g = -1.0$) and attractive HOI ($\sigma \leq 0$) for runs up to $t = 100$. The plot shows the unstable space-time evolution of the wave for $\sigma = -0.25$ and $V_s = 1.0$.

We launch numerical computations for the case of BECs, with *attractive* two-body interactions ($g = -1$), trapped in both harmonic and optical fields. As is known from previous works, such condensate is dynamically unstable for most wave numbers in the absence of OL and HOI. Here, we show that the stability of the system dramatically changes when the optical potential is switched on in the presence of HOI.

Fig. 9 portrays the 3D evolution of the wave in time and space for negative HOI parameter ($\sigma = -0.25$). We realize that an exponential growth arises in the amplitude of the wave. As we see the amplitude square can easily go from 1.0 to about 6.5, which means that the system is dynamically unstable. The four middle OL wells which are located in the inner region of the MT are more affected by MI than the outer wells. However, as we observed, the instability may expand to OL wells in the outer region of the MT as the OL strength (or the HOI) increases. Thus the attractive two-body and HOI are dynamically destabilizing for the condensate, and the OL strength cannot help suppressing such instability.

When the HOI becomes repulsive, the OL strength starts playing an active part in reducing the instability. Fig. 10 shows the 3D evolution of the wave in time and space for positive HOI parameter ($\sigma = +1.0$) for two different values of the OL parameter. Panel (a) shows the case of big OL strength ($V_s > 4.0$), while panel (b) corresponds to smaller OL strength ($V_s < 4.0$).

In the case of deep OL wells as displayed in panel (a), the wave amplitude slightly increases from 1.0 to about 1.5, small compared to the previous case in Fig. 9. So the exponential growth does not arise in the amplitude of the wave, which means that the system is dynamically

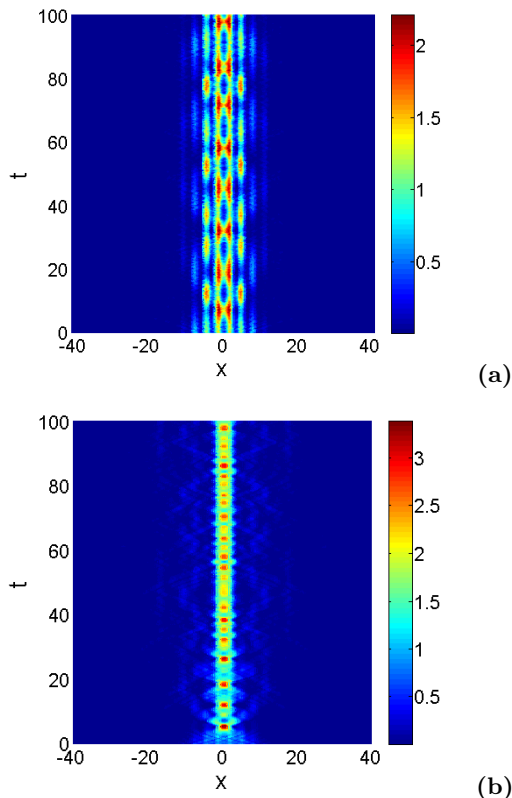


FIG. 10: Numerical dynamics of the wave in the system with two-body attraction ($g = -1.0$) and repulsive HOI ($\sigma = +1.0$) for runs up to $t = 100$ and for (a) $V_s > 4.0$, and (b) $V_s < 4.0$. The plot in panel (a) depicts the stable space-time evolution of the wave when $V_s = 6.0$. Panel (b) shows the unstable space-time evolution of the wave when $V_s = 1.5$.

stable. In all OL wells, the amplitude exhibits mild oscillations with equal frequency which do not move the system away from its initial state. Oscillations in the outer region are out of phase with that in the inner region. A strong breathing behavior of the wave in the system is clearly seen. The OL strength has a perceptible effect on the instability of the system. As displayed in panel (b), decreasing the depth of OL wells for instance from 6.0 to 1.5 destabilizes the system. The wave amplitude grows quickly and, simultaneously, a strong localization of the wave occurs in the center of the OL. So when the two-body interaction is attractive and the HOI repulsive, the higher OL strength reduces or prevents the growth of the wave amplitude in the system, and thus can help suppressing dynamical instability in the condensate.

Hence, with two-body attraction in the condensate, the system is dynamically stable when $\sigma > 0$ and $V_s > 4$. This stability is improved for sufficiently large values of

the HOI parameter σ .

V. CONCLUSION

In summary, we have analytically and numerically discussed the dynamical instability of Bose-Einstein condensates with HOI trapped in parabolic potential embedded in an OL. Through the time dependent variational approach, we have obtained the set of ordinary differential equations that govern the evolution of the perturbation in the system. Moreover, we have established the criterion that defines the onset of dynamical instability in the condensate. This work points out the effect of OL depth and HOI strength in the dynamical stability of the system.

When the two-body interaction is repulsive, the condensates can be unstable. This occurs whether the HOI is attractive or repulsive. When the HOI is attractive, the instability is oscillatory, consisting of the scattering of the wave envelope in space, and occurs for OL strengths $V_s \leq -2q^2$. When the HOI is repulsive, the instability is clearly dynamical and manifests itself through an exponential growth in the wave amplitude. In this case, increasing the strength of the HOI interaction enhances the instability in the system.

When the two-body interaction is attractive, the condensates can be dynamically stable. This occurs when the HOI is repulsive and the OL wells deep enough. In all OL wells, owing to that stability, there is neither exponential growth nor scattering of the wave envelope. The wave amplitude benignly oscillates around its initial value. The oscillations in the outer region are out of phase with the oscillations in the inner region of the trap. This is a clear proof that the system is dynamically stable. Besides, reducing the depth of OL wells gives rise to the dynamical instability in the system, clearly characterized by a strong localization and growth of wave amplitude.

Acknowledgments

S.S. thanks the Department of Science and Technology (DST) for fellowship grant. KP acknowledges DST, IFCPAR, DST-FCT and CSIR, the Government of India, for financial support through major projects. AM thanks the Abdus Salam ICTP for financial support through the Associateship program.

References

-
- [1] B.P. Anderson and M.A. Kasevich, Science **282**, 1686 (1998).
 - [2] E.W. Hagley, L. Deng, M. Kozuma, J. Wen, K. Helmer-

- son, S.L. Rolston, and W.D. Phillips, *Science* **283**, 1706 (1999).
- [3] B. Eiermann, Th. Anker, M. Albiez, M. Taglieber, P. Treutlein, K.-P. Marzlin, and M.K. Oberthaler, *Phys. Rev. Lett.* **92**, 230401 (2004).
- [4] K. Berg-Sørensen and K. Mølmer, *Phys. Rev. A* **58**, 1480 (1998).
- [5] D.-I. Choi and Q. Niu, *Phys. Rev. Lett.* **82**, 2022 (1999).
- [6] B.A. Malomed, Z.H. Wang, P.L. Chu, and G.D. Peng, *J. Opt. Soc. Am. B* **16**, 1197 (1999).
- [7] M.A. Porter and P. Cvitanović, *Phys. Rev. E* **69**, 047201 (2004).
- [8] F.S. Cataliotti, S. Burger, C. Fort, P. Maddaloni, F. Minardi, A. Trombettoni, A. Smerzi, and M. Inguscio, *Science* **293**, 843 (2001).
- [9] O. Morsch, J.H. Müller, M. Cristiani, D. Ciampini, and E. Arimondo, *Phys. Rev. Lett.* **87**, 140402 (2001).
- [10] M. Cristiani, O. Morsch, J.H. Müller, D. Ciampini, and E. Arimondo, *Phys. Rev. A* **65**, 063612 (2002).
- [11] B. Wu and Q. Niu, *New J. Phys.* **5**, 104 (2003).
- [12] B. Eiermann *et al.*, *Phys. Rev. Lett.* **91**, 060402 (2003).
- [13] M. Greiner, O. Mandel, T. Esslinger, T.W. Hansch, and I. Bloch, *Nature (London)* **415**, 39 (2002).
- [14] B. Wu, R.B. Diener, and Q. Niu, *Phys. Rev. A* **65**, 025601 (2002).
- [15] G.P. Zheng, J.Q. Liang, and W.M. Liu, *Phys. Rev. A* **71**, 053608 (2005).
- [16] Z.W. Xie, Z.X. Cao, E.I. Kats, and W.M. Liu, *Phys. Rev. A* **71**, 025601 (2005).
- [17] Z.D. Li, P.B. He, L. Li, J.Q. Liang, and W.M. Liu, *Phys. Rev. A* **71**, 053611 (2005).
- [18] F. Dalfovo, S. Giorgini, L.P. Pitaevskii, and S. Stringari, *Rev. Mod. Phys.* **71**, 463 (1999).
- [19] T. Köhler, K. Góra, and P.S. Julienne, *Rev. Mod. Phys.* **78**, 1311 (2006).
- [20] F.Kh. Abdullaev, B. Baizakov, S. Darmanyan, V.V. Konotop, and M. Salerno, *Phys. Rev. A* **64**, 043606 (2001).
- [21] I. Carusotto, D. Embiraco, and G.C. La Rocca, *Phys. Rev. A* **65**, 053611 (2002).
- [22] P.J.Y. Louis, E.A. Ostrovskaya, C.M. Savage, and Y.S. Kivshar, *Phys. Rev. A* **67**, 013602 (2003).
- [23] O. Morsch, and M. Oberthaler, *Rev. Mod. Phys.* **78**, 179 (2006).
- [24] L. Khaykovich, F. Schreck, G. Ferrari, T. Bourdel, J. Cubizolles, L.D. Carr, Y. Castin, and C. Salomon, *Science* **296**, 1290 (2002).
- [25] S.L. Cornish, S.T. Thompson, and C.E. Wieman, *Phys. Rev. Lett.* **96**, 170401 (2006).
- [26] G.L. Alfimov, V.V. Konotop, and M. Salerno, *Europhys. Lett.* **58**, 7 (2002).
- [27] L. Salasnich, A. Cetoli, B.A. Malomed, and F. Toigo, *Phys. Rev. A* **75**, 033622 (2007).
- [28] N.T. Zinner and M. Thøgersen, *Phys. Rev. A* **80**, 023607 (2009).
- [29] L. De Sarlo, L. Fallani, J.E. Lye, M. Modugno, R. Saers, C. Fort, and M. Inguscio, *Phys. Rev. A* **72**, 013603 (2005).
- [30] G.P. Agrawal, *Nonlinear Fiber Optics* (San Diego, CA:Academic) (2001).
- [31] V.V. Konotop and M. Salerno, *Phys. Rev. A* **65**, 021602(R) (2002).
- [32] L. Fallani, L. DeSarlo, J.E. Lye, M. Modugno, R. Saers, C. Fort, and M. Inguscio, *Phys. Rev. Lett.* **93**, 140406 (2004).
- [33] G. Barontini and M. Modugno, *Phys. Rev. A* **76**, 041601(R) (2007).
- [34] K.E. Strecker, G.B. Partridge, A.G. Truscott, and R.G. Hulet, *Nature* **417**, 150 (2002).
- [35] K.E. Strecker, G.B. Partridge, A.G. Truscott, and R.G. Hulet, *New J. Phys.* **5**, 73 (2003).
- [36] F.S. Cataliotti *et al.*, *New J. Phys.* **5**, 71 (2003).
- [37] A. Smerzi, A. Trombettoni, P.G. Kevrekidis, and A.R. Bishop, *Phys. Rev. Lett.* **89**, 170402 (2002).
- [38] G. Theocharis, Z. Rapti, P.G. Kevrekidis, D.J. Frantzeskakis, and V.V. Konotop, *Phys. Rev. A* **67**, 063610 (2003).
- [39] P.G. Kevrekidis, G. Theocharis, D.J. Frantzeskakis, and A. Trombettoni, *Phys. Rev. A* **70**, 023602 (2004).
- [40] J.S. Huang, Z.W. Xie, M. Zhang and L.F. Wei, *J. Phys. B: At. Mol. Opt. Phys.* **43**, 065305 (2010).
- [41] Z. Rapti, P.G. Kevrekidis, A. Smerzi, and A.R. Bishop, *J. Phys. B: At. Mol. Opt. Phys.* **37**, S257 (2004).
- [42] J. Ruostekoski and Z. Dutton, *Phys. Rev. A* **76**, 063607 (2007).
- [43] K. Kasamatsu and M. Tsubota, *Phys. Rev. Lett.* **93**, 100402 (2004).
- [44] W.X. Zhang, D.L. Zhou, M.S. Chang, M.S. Chapman, and L. You, *Phys. Rev. Lett.* **95**, 180403 (2002).
- [45] P.G. Kevrekidis, R. Carretero-González, G. Theocharis, D.J. Frantzeskakis, and B.A. Malomed, *Phys. Rev. A* **68**, 035602 (2003).
- [46] K. Kasamatsu and M. Tsubota, *Phys. Rev. A* **74**, 013617 (2006).
- [47] A. Smerzi, A. Trombettoni, P.G. Kevrekidis, and A.R. Bishop, *Phys. Rev. Lett.* **89**, 170402 (2002).
- [48] A. Fabrocini, A. Polls, *Phys. Rev. A* **60**, 2319 (1999).
- [49] H. Fu, Y. Wang, B. Gao, *Phys. Rev. A* **67**, 053612 (2003).
- [50] A. Collin, P. Massignan, and C.J. Pethick, *Phys. Rev. A* **75**, 013615 (2007).
- [51] J.J. García-Ripoll, V.V. Konotop, B. Malomed, V.M. Pérez-García, *Math. Comput. Simul.* **62**, 21 (2003).
- [52] F. Kh. Abdullaev and M. Salerno, *Phys. Rev. A* **72**, 033617 (2005).
- [53] A.-X. Zhang and J.-K. Xue, *Phys. Rev. A* **75**, 013624 (2007).
- [54] W. Zhang, E.M. Wright, H. Pu, and P. Meystre, *Phys. Rev. A* **68**, 023605 (2003).
- [55] E. Wamba, K. Porsezian, A. Mohamadou, and T.C. Kofané, *Phys. Lett. A* **377**, 262 (2013).
- [56] S. Sabari, E. Wamba, K. Porsezian, A. Mohamadou, and T.C. Kofané, *Phys. Lett. A* **377**, 2408 (2013).
- [57] E. Wamba, A. Mohamadou, and T.C. Kofané, *Phys. Rev. E* **77**, 046216 (2008).
- [58] E. Wamba, A. Mohamadou, and T.C. Kofané, *J. Phys. B: At. Mol. Opt. Phys.* **41**, 225403 (2008).
- [59] S. Sabari, R.V.J. Raja, K. Porsezian, and P. Muruganandam, *J. Phys. B: At. Mol. Opt. Phys.* **43**, 125302 (2010).
- [60] X.-Y. Qi and J.-K. Xue, *Phys. Rev. E* **86**, 017601 (2012).